5

Mitigation of SHC-ripple in the DC-DC-AC Converter: An ISM Based Control Approach

Recently several classical control methods are applied and researched for the mitigation of second-order harmonic ripple. The dual-loop control is one of the conventional classical control methods to mitigate the SHC ripple problem in two-stage DC-DC-AC converters. The concept of the ripple reduction at input is based on the bandwidth-shaping. To achieve ripple-reduction at the input, the two bandwidths are separated atleast half decade from the SHC ripple frequency, generally, the bandwidth of the voltage loop is kept very low. The challenge of this method is the sluggish transient operation of the system due to the low bandwidth of voltage loop. To solve this problem, some methods are available in the existing literature (see Chapter Two). The classical control such as PID, optimal control performs well at the operating point, however, these control compromises among the dynamic performance, robustness and stability at the large line-load transients. Moreover, the actual power converters are subjected to disturbances or uncertainty in the system such as parametric variations, exogenous disturbances, sensor's noise and disturbances caused by magnetic components, unmodeled system dynamics. The nonlinear control approaches are better choice in the systems having frequent large line-load transients and uncertainty in the system parameters. Therefore, there is a need of control techniques which combine the merits of the classical control and modern non-linear control. The integral sliding mode (ISM) control is one of the nonlinear robust control approaches [Loukianov *et al.*, 2006; Rubagotti *et al.*, 2011]. Many researches have proposed integral sliding surfaces, however, ISM control is substantially different than these surfaces. In ISM control, the dynamic performance is guaranteed by nominal controller and ISM controller rejects only disturbances. The nominal controller can be designed by any methodology i.e. PI, optimal, H_∞; the ISM control methodology adds a nonlinear controller to the nominal controller and thus overall control law is obtained. The combined control is robust and possesses invariance property against the matched uncertainty [Utkin and Shi, 1996]. Furthermore, the nominal classical control such as conventional dual-loop control method minimizes the SHC ripple at the input for the nominal and normal operating conditions only. In the abnormal conditions such as parametric variations, the ripple may proliferate at the input. An ISM based controller eliminates the SHC ripple at the input along with other exogenous disturbances matched to the control input. In the literature, to the best of authors knowledge, the application of the classical control in conjunction with the ISM based control is not addressed for the SHC ripple-mitigation in particular. This is the motivation behind the proposed ISM based controller.

This Chapter presents an integral sliding mode based controller for the two-stage DC-DC-AC converter to mitigate the SHC ripple along with desired dynamic performance. The Chapter is organized as follows. The dynamic modeling of the system is discussed in the Section 5.1. A linear dynamic model is developed to design PI controllers for the dual-loop control scheme. The Section 5.2 presents concept of SHC ripple reduction using dual-loop control method. In Section 5.3, the proposed ISM based controller is discussed. In this Section, a new adaptive PI controller as the nominal controller for the ISM control is proposed. The adaptive nature of the nominal controller mitigates the SHC ripple and improves the dynamic performance of the system. Moreover, the ISM based controller (with nominal PI controllers in the dual-loop control) eliminates uncertainty/disturbances matched to the control input. This Section also discusses about the ex-

istence condition of the sliding mode and stability of the system. Furthermore, a design example is presented to design the proposed ISM based controller. In Section 5.4 and Section 5.5, the simulation results using MATLAB-Simulink and hardware results are presented respectively for an 1 kW-system. Section 5.6 summarizes the Chapter Five.

5.1 DYNAMIC MODEL OF THE SYSTEM

A circuit of the boost-derived two-stage DC-DC-AC converter is shown in Fig. 5.1(a). For the simplicity the inverter is considered as a current source. The simplified circuit is shown in the Fig. 5.1(b).

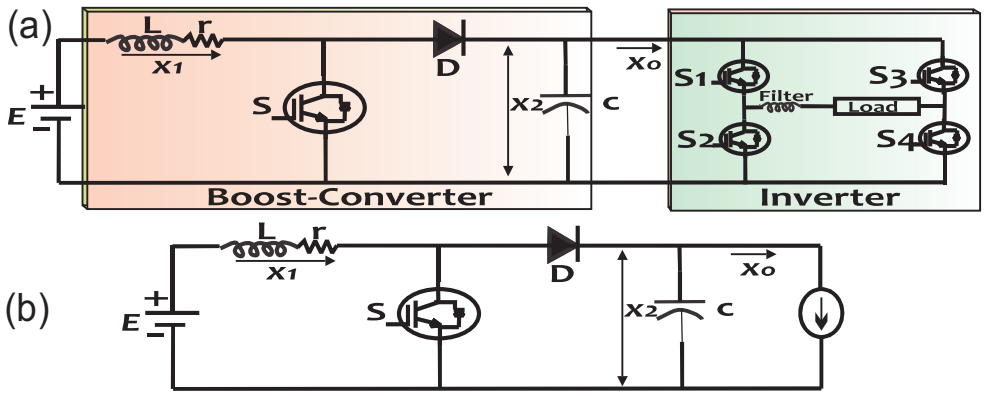

Figure 5.1 : (a) Circuit of two-stage DC-DC-AC converter (b) equivalent circuit

The dynamic model of the circuit of Fig. 5.1(b),

$$\dot{x}(t) = f(x(t)) + g(x(t))u \tag{5.1}$$

Here, $f(x(t)) = [\frac{E-rx_1-x_2}{L} \quad \frac{x_1-x_o}{L}]^\intercal$ and $g(x(t)) = [\frac{x_2}{L} \quad -\frac{x_1}{C}]^\intercal$, $\intercal$ stands for transpose. E is input voltage, x_1 is the inductor/input current, x_2 is the DC-link voltage, x_o is the DC-link current/input current of the inverter. u is the control input. L and C are the inductance and capacitance respectively. It is to be noted that the proposed ISM based controller implements a dual-loop control using new proposed adaptive PID controllers as a nominal controller. To design PID-controller, a linear dynamic model is developed using small-signal perpetuation method. The perturbed state-variables are $x_1 = x_{1r} + \tilde{x}_1$, $x_2 = x_{2r} + \tilde{x}_2$, $E = E_o + \tilde{E}$, $u = D_0 + d$. Here $(\tilde{})$ represents the small-signal value. d is also perturbed value of the duty. For small-signal modeling, $x_o = \frac{x_2}{Z_o}$ is replaced by a fixed load. Z_o is the constant load at DC-link. x_{1r}, x_{2r}, D_0, E_o are the operating or steady-state values. Using perturbed variables in (5.1) and collecting only AC terms gives small signal mode. The small-signal dynamic model is as follows,

$$\begin{bmatrix} \dot{\tilde{x}}_1 \\ \dot{\tilde{x}}_2 \end{bmatrix} = \begin{bmatrix} -\frac{r}{L} & -\frac{(1-D_0)}{L} \\ \frac{(1-D_0)}{C} & -\frac{1}{CZ_o} \end{bmatrix} \begin{bmatrix} \tilde{x}_1 \\ \tilde{x}_2 \end{bmatrix} + \begin{bmatrix} \frac{x_{2r}}{L} \\ -\frac{x_{1r}}{C} \end{bmatrix} d + \begin{bmatrix} \frac{\tilde{E}}{L} \\ 0 \end{bmatrix} \tag{5.2}$$

Some of the useful transfer functions used to design the nominal controller are given here. These transfer functions are derived using the Laplace-transform of (5.2).

1) Control input to DC-link voltage

$$G_{vd}(s) = \frac{\tilde{x_2}(s)}{d(s)}|_{\tilde{E}(s)=0} = \frac{(1-D_0)x_{2r} - (sL+r)x_{1r}}{LCs^2 + (\frac{L}{Z_o} + rC)s + \frac{r}{Z_o} + (1-D_0)^2}$$

2) Control input to inductor current

$$G_{cd}(s) = \frac{\tilde{x_1}(s)}{d(s)}|_{\tilde{E}(s)=0} = \frac{sCx_{2r}+2(1-D_0)x_{1r}}{LCs^2+(\frac{L}{Z_o}+rC)s+\frac{r}{Z_o}+(1-D_0)^2}$$

3) Inductor current to DC link voltage

$$G_{vc}(s) = \frac{\tilde{x_2}(s)}{\tilde{x_1}(s)}|_{\tilde{E}(s)=0,d(s)=0} = \frac{(1-D_0)x_{2r}-(sL+r)x_{1r}}{Cx_{2r}s+2(1-D_0)x_{1r}}$$

Before proceeding for the proposed adaptive PID-controller design, the effect of the loop-bandwidth(s) on the SHC ripple and system dynamics are discussed in the next Section.

5.2 DUAL-LOOP CONTROL FOR SHC RIPPLE MINIMIZATION

The loop-bandwidth shaping in the multi-loop control method plays an important role to achieve desired system performance such as, line-load transients, overshoot/undershoot, system response time, attenuation of the high/low frequency ripple and other system characteristics. Generally, the capacitor voltage dynamics are comparatively slower than the inductor current dynamics. Therefore, in dual-loop control method, the current-loop is chosen the inner-loop and voltage-loop is chosen the outer-loop. Also, this is why, the inductor current reference is generated using voltage error. It is to be noted that 2ω-ripple is a main concern here. According to Liu and Lai [2007b], if the interaction between the inner-loop and outer-loop in a dual-loop control method applied to the front-end converter is avoided such that the bandwidths of two-loops remain well separated from the SHC ripple frequency, in such case, the ripple-reduction at DC input can be achieved. For this, atleast half-decade separation between two loops is required.

5.2.1 Dual-loop PID Controller Design

In Fig. 5.2, a block diagram of dual-loop control method for the circuit in Fig. 5.1 is shown.

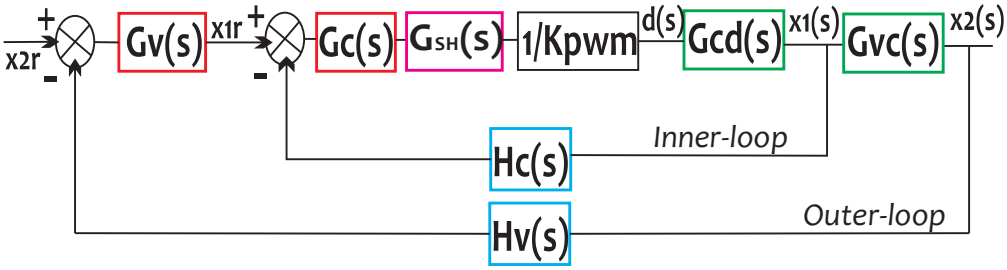

Figure 5.2 : Block diagram of dual-loop control

In the Fig. 5.2, the loop-gain of current-loop and loop-gain of voltage-loop are,

1) Loop-gain of current-loop

$$T_c(s) = \frac{G_{SH}(s)G_c(s)G_{cd}(s)H_c(s)}{K_{pwm}} \tag{5.3}$$

2) Loop-gain of voltage-loop

$$T_v(s) = \frac{Gv(s)G_{SH}(s)G_c(s)H_v(s)G_{cd}(s)G_{vc}(s)}{K_{pwm} + G_{SH}(s)G_cH_c(s)G_{cd}(s)} \tag{5.4}$$

In (5.3) and (5.4), $G_{SH}(s) = \frac{1-exp(-sT_s)}{s}$ is the computational sample and hold time delay. T_s is the sampling rate. The approximated linear time delay is given by $G_{SH}(s) = \frac{1}{1+0.5sT_s}$ Duan and Jin [1999]. In Fig. 5.3, the Bode plots of loop gains of current-loop and voltage-loop for $G_v(s) = G_c(s) = 1$ are shown using nominal values given in Table 5.1.

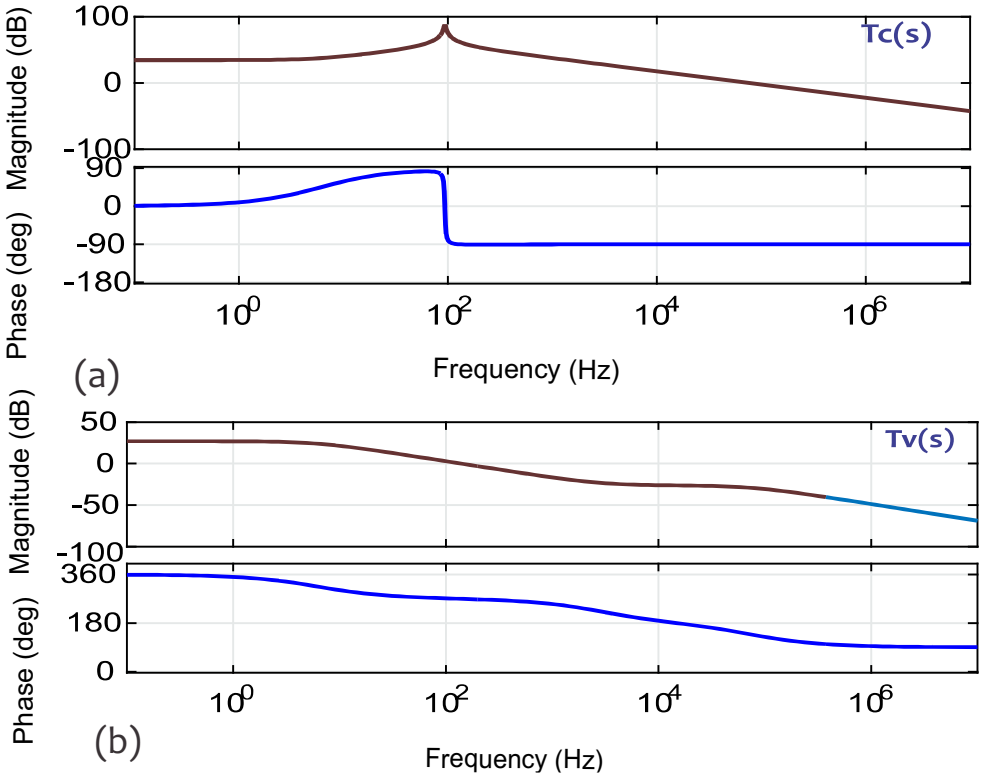

Figure 5.3 : Block diagram of (a) current loop gain and (b) voltage loop gain for $G_v(s) = G_c(s) = 1$

From the Fig. 5.3, it is evident that there is a need of improvement of low frequency gain to reduce steady-state error, improvement of phase margin for better transient performance and high frequency attenuation to eliminate the noise, which is why the following steps are used to design PID controller Liu and Lai [2007b],

Step-1: Integral action of a pole at origin eliminates steady-state error. Therefore, place a pole at the origin.

Step-2: To attenuate the high frequency noise or ripple, place a pole at half of the switching frequency (f_s).

Step-3: To minimize the overshoot, place a zero at or below the resonance frequency (f_o) of the converter.

The above three steps are the common steps for the PID controller design of the inner and outer loops. The final step of this design is to shape the bandwidths of inner-loop and outer-loop by choosing suitable value of the gains. It is to be noted that this particular step is important to mitigate

$2\omega-$ripple problem and will be discussed under the Section 5.4. Suppose the k_c and k_v are the gains of the current controller and voltage controller respectively. The PID-controllers for inner loop and outer loop are,

$$G_c(s) = \frac{k_c(1+\frac{1}{2\pi f_o}s)}{s(1+\frac{1}{\pi f_s}s)} \tag{5.5a}$$

$$G_v(s) = \frac{k_v(1+\frac{1}{2\pi f_o}s)}{s(1+\frac{1}{\pi f_s}s)} \tag{5.5b}$$

Suppose the desired cross-over frequency (or bandwidth) of the current-loop gain and the desired cross-over frequency of the voltage-loop gain are f_c and f_v respectively. In (5.3) and (5.4), the only unknown are the value of k_c in $G_c(s)$ and the value of k_v in $G_v(s)$ respectively. However, $|T_c(2\pi f_c)| = 1$ and $|T_v(2\pi f_v)| = 1$. Solving these give the values of gains (k_c, k_v) corresponding to desired cross-over frequencies.

In the conventional dual-loop control, the values of f_v and f_c are kept fixed such that $f_v << f_c$, therefore the dynamics performance of system is poor. The readers are advised to see Section 5.4.1; a detailed analysis of conventional dual-loop control for ripple mitigation and its drawback is discussed under the Section 5.4 through simulation results. To improve the performance of conventional dual-loop control, a new adaptive PID control for dual-loop method is discussed in the next Section.

5.3 PROPOSED ISM BASED CONTROLLER

The proposed control amalgamates an adaptive dual-loop PID-control as a nominal controller and the sliding mode control. The voltage-loop controller is an adaptive PID-controller unlike the dual-loop control method of Liu and Lai [2007b] in which ripple reduces but at the cost of the poor system dynamics. The adaptive nature of the proposed PID-controller improves the method used in Liu and Lai [2007b] by enhancing the dynamic performance of the system.

5.3.1 Adaptive PID Controller

The central idea of the proposed adaptive PID-controller in dual-loop control is to self tune or shape the bandwidth of voltage-loop. This is achieved by designing k_v as a function of DC-link voltage, x_2. At the steady-state, k_v remains low, this implies low bandwidth of voltage-loop at the steady-state. At the line-load transients, the value of k_v increases monotonically, this increases the bandwidth of the voltage-loop and make the convergence of the system dynamics at a faster rate. As the system dynamics converges, the bandwidth of the voltage-loop becomes low again. This makes an adaptive nature of the proposed PID-controller. It is to be noted that the bandwidth of the current-loop is kept fixed and comparatively large such that the interaction between inner and outer loop is avoided at the steady-state Liu and Lai [2007b]. The control of the SHC ripple at the input and dynamic performance of the system are handled by the adaptive nature of the outer-loop bandwidth. For this, the voltage-loop gain is defined as,

$$k_v(x_2) := sat[\zeta exp(\frac{x_{2l}-x_2}{x_{2u}-x_2})]_{\beta_l}^{\beta_u} \tag{5.6}$$

Here, exp is for exponential function and sat is for saturation. β_l and β_u are the lower bound and upper bound of the function under the square brackets. x_{2l} and x_{2u} are the allowed voltage variations in x_2 at the steady-state. ζ is the limiting value of function under braces. For the $R\%$ voltage regulation at DC-link, $x_{2l} = (1-\frac{R\%}{100})x_{2r}$ and $x_{2u} = (1+\frac{R\%}{100})x_{2r}$. A design example of the k_v is presented in the Section 5.3.5.

The PID-control is susceptible to the parametric variations, exogenous disturbances, unmodeled dynamics and sensor's noise. These factors may disturb the control and shift the actual operating points or may cause unwanted perturbation in the system states. A large variation in the system parameters may induce instability to the system. Also, the boost converter has a bilinear system dynamics. The linearisation of such system dynamics ignores the non-linear terms. This may results in an inadequate information communicated to the controller. Also, SHC ripple is a low frequency disturbance. These disturbances may affect the nominal control input. Therefore, an ISM based controller is designed further using the proposed nominal adaptive PID control to eliminate the matched uncertainty/disturbances.

5.3.2 ISM based Controller (The Overall Control)

The basic form of the integral switching function is Utkin and Shi [1996],

$$\sigma(x(t)) = G[x(t) - x(0) - \int_0^t \{f(x(\tau)) + g(x(\tau))u_o(x(\tau))\}\, d\tau] \tag{5.7}$$

Here, G is a matrix to be designed. $x(0)$ is the initial condition. u_0 is the control input of nominal controller. The total control input (u) is,

$$u = u_o + u_n \tag{5.8}$$

Here u_n is the discontinuous control input of SMC. u_n induces the sliding motion in the system and u_o helps in maintaining the sliding mode.

In (5.7), at $t = 0$, $\sigma(x(0)) = 0$. Hence, from the initial time instance, the system states are at sliding surface that implies that the reaching-phase is eliminated and hence the matched uncertainty eliminates.

5.3.3 Existence of Sliding Mode

The choice of the integral switching function given by (5.7) ensures that the sliding mode begins at $t = 0$. The $\eta-$readability condition given by (5.9) is analyzed here.

$$\sigma(x(t))\dot{\sigma}(x(t)) = -\eta|\sigma(x(t))| \tag{5.9}$$

For this, consider a Lyapunov function as,

$$V = \frac{\sigma(x(t))^2}{2} \tag{5.10}$$

The time-derivative of V gives,

$$\dot{V} = \sigma(x(t))\dot{\sigma}(x(t)) \tag{5.11}$$

The time derivative of (5.7) gives,

$$\dot{\sigma}(x(t)) = G\dot{x}(t) - G\{f(x(t)) + g(x(t))u_o\} \tag{5.12}$$

Using (5.12) in (5.11),

$$\dot{V} = \sigma(x(t))[G\dot{x}(t) - G\{f(x(t)) + g(x(t))u_o\}] \tag{5.13}$$

Using (5.1) and (5.13),

$$\dot{V} = \sigma(x(t))\{Gg(x(t))(u-u_o)\} \tag{5.14}$$

Substituting (5.8) in (5.14),

$$\dot{V} = \sigma(x(t))\{Gg(x(t))u_n\} \tag{5.15}$$

one of the choices of discontinuous control (u_n) in (5.8) is $u_n = -\eta(Gg(x(t)))^{-1}sign(\sigma)$. This gives,

$$\dot{V} = -\eta\sigma(x(t))sign(\sigma(x(t))) \tag{5.16a}$$
$$\dot{V} = -\eta|\sigma(x(t))| \tag{5.16b}$$

Here, $|\sigma(x(t))| = \sigma(x(t))sign(\sigma(x(t)))$. To satisfy $\dot{V} < 0$, in (5.16), η must be a positive number. Hence, by design $\eta > 0$. This ensures $\eta-$ reachability condition.

5.3.4 Stability

In the integral sliding mode control, the system dynamics are governed by the nominal controller. Therefore, the stability of the sliding mode depends on the stability of the nominal controller. The voltage-loop gain i.e. given by (5.4) is the overall loop transfer function. Using (5.4), the stability of the system can be investigated. Using (5.4), the gain-margin (GM) and phase-margin (PM) can be obtained to do analysis on the stability of the system. The minimum value of the gain margin (GM) should be $GM = \frac{1}{|Tcv(2\pi f_{180^0})|} > 6\ dB$ and the minimum value of the phase-margin (PM) should be $PM = 180^0 + \angle T_v(2\pi f_{gc}) > 30^0$ for the good working of the system, here f_{gc} is gain cut-off frequency. The design of the stability margins is covered in the next subsection.

5.3.5 Design Example

Firstly, the design of proposed adaptive-PID control in dual-loop is discussed and thereafter, the design of ISM-based control is presented using proposed adaptive PID control.

Design of Adaptive $-$ PID control : Suppose the system parameters $E, x_{2r}, x_{1r}, Z_o, D_0, L, C, r, f_s$,

H_v, H_c, K_{pwm} in Fig. 5.2 are known, then the design for adaptive PID control is as follow,

1) Design of current controller gain, (k_c): Using G_{cd}, the resonance frequency (f_o) is calculated. Solving $|G_{cd}(2\pi f)|$ for the maximum value gives the value of f_o. The bandwidth of the current-loop should be kept between $f_s/20$ to $f_s/10$ to eliminate the high frequency. Using (5.5a), the inner-loop PID-controller $G_c(s)$ is designed. The only unknown in $G_c(s)$ is k_c. The value of the k_c is calculated using (5.3). Solving $|T_c(2\pi f_c)| = 1$ gives the value of k_c.

2) Design of voltage controller gain, (k_v): It is to be noted that the small size of the voltage-loop bandwidth causes sluggish response of the system dynamics. A faster response can be achieved by decreasing the GM of the system. However, for the proper working of the system the GM should be atleast 6 dB and PM should be atleast 30^0. Considering this, for a fixed value of k_c, a range of k_v can be calculated using (5.4). Therefore, the maximum and minimum values of k_v in (5.6) are obtained using (5.4). The value of the k_v changes monotonically between the minimum and maximum values. In (5.6), as soon as the x_2 departs from the 5% voltage regulation range at line-load transients, the value of the k_v increases. The value of k_v decreases to initial value again, as soon as the system dynamics converges. For the system parameters given in the Table 5.1, a bode plot using (5.4) is shown in the Fig. 5.4. The maximum value of k_v is 7068. For $k_v \leq 0.075$, the system have a constant PM of 90^o and enough GM also. The values of β_u and β_l in (5.6) can be chosen based on these limits of k_v.

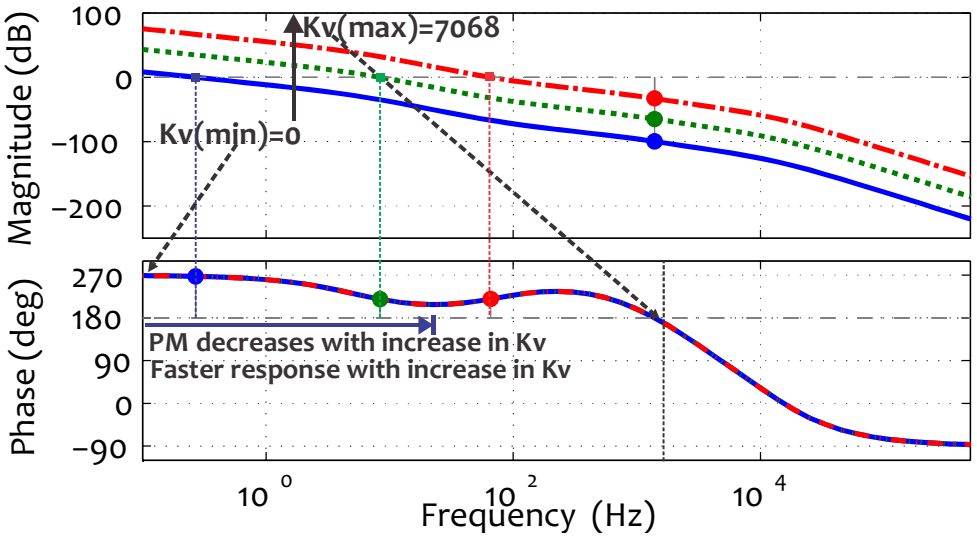

Figure 5.4 : Bode plot of overall system $T_v(s)$

Design of ISM based control : The dynamic model given by (5.1) is simplified as follows,

$$\dot{x}(t) = Z\{f_1(x(t)) + g_1(x(t))u\} \tag{5.17}$$

Here, $f_1(x(t))$ and $g_1(x(t))$ are function of x and t such that,

$$x(t) := \begin{bmatrix} x_1 \\ x_2 \end{bmatrix},\ f_1(x(t)) := \begin{bmatrix} E - rx_1 - x_2 \\ x_1 - x_o \end{bmatrix}$$

$$g_1(x(t)) := \begin{bmatrix} x_2 \\ -x_1 \end{bmatrix},\ Z := \begin{bmatrix} z_1 & 0 \\ 0 & z_2 \end{bmatrix},\ z_1 = \frac{1}{L},\ z_2 = \frac{1}{C}$$

Suppose the SHC ripple, as a disturbance, causes perturbation in state-variables. This implies $E,\ x_1,\ x_2,\ x_o,\ u$ changes to

$$E + \Delta E,\ x_1 + \Delta x_1,\ x_2 + \Delta x_2,\ x_o + \Delta x_o,\ u + \Delta u$$

respectively. Also, the system parameters vary from their nominal values, say Z changes by ΔZ, this implies z_1 changes to $z_1 + \Delta z_1$ and z_2 changes to $z_2 + \Delta z_2$. Substituting perturbed variables in (5.17) gives,

$$\dot{x}(t) = Zf_1(x(t)) + Zg_1(x(t))u + \varphi(x(t)) \tag{5.18}$$

Here, $\varphi(x(t))$ is the disturbance given by $[Z\Delta g_1(x(t)) + \Delta Z g_1(x(t)) + \Delta Z \Delta g_1(x(t))]u + [Z\Delta f_1(x(t)) + \Delta Z(f_1(x(t)) + \Delta f_1(x(t))) + (Zg_1(x(t)) + Z\Delta g_1(x(t)) + \Delta Z g_1(x(t)) + \Delta Z \Delta g_1(x(t)))\Delta u]$. The part of $\varphi(x(t))$ i.e. $[Z\Delta g_1(x(t)) + \Delta Z g_1(x(t)) + \Delta Z \Delta g_1(x(t))]u$ contains the ripple component and parametric uncertainty and is a matched uncertainty available explicitly to designer. However, there may be other matched and unmatched uncertainty in the system, to find those uncertainties one may follow the procedure below,

The disturbance $\varphi(x(t))$ is a column vector contains the matched disturbance (say, $\varphi_m(x(t))$) and unmatched disturbance (say, $\varphi_u(x(t))$). A general approach to separate the matched disturbances and unmatched disturbances is as follows Rubagotti *et al.* [2011],

$$\varphi_m(x(t)) \triangleq g(x(t))g^+(x(t))\varphi(x(t)) \tag{5.19a}$$

$$\varphi_u(x(t)) \triangleq g^\perp(x(t))g^{\perp+}(x(t))\varphi(x(t)) \tag{5.19b}$$

Here, superscript $\perp$ is the symbol for orthogonal complement (in short *perp*) and superscript $+$ is operator for left pseudo-inverse. This means $g^+(x(t)) = \{g^\intercal(x(t))g(x(t))\}^{-1}g^\intercal(x(t))$ and $g^{\perp+}(x(t)) = \{g^{\perp\intercal}(x(t))g^\perp(x(t))\}^{-1}g^{\perp\intercal}(x(t))$. Using these in (5.18),

$$\begin{aligned}\dot{x}(t) = f(x(t)) + g(x(t))u + g(x(t))g^+(x(t))\varphi(x(t)) + \\ g^\perp(x(t))g^{\perp+}(x(t))\varphi(x(t))\end{aligned} \tag{5.20}$$

Here $f(x(t)) = Zf_1(x(t))$ and $g(x(t)) = Zg_1(x(t))$. The sliding motion is governed by equivalent controller. Therefore, the equivalent controller is enforced at sliding mode. This implies $\dot{\sigma}(x(t))) = 0$. For this consider the derivative of (5.7),

$$\dot{\sigma}(x(t)) = G\dot{x}(t) - G\{f(x(t)) + g(x(t))u_o\} \tag{5.21}$$

Using (5.20) in (5.21),

$$\begin{aligned}\dot{\sigma}(x(t)) = Gg(x(t))u + Gg(x(t))g^+(x(t))\varphi(x(t)) + \\ Gg^\perp(x(t))g^{\perp+}(x(t))\varphi(x(t)) - Gg(x(t))u_o\end{aligned} \tag{5.22}$$

Solving $\dot{\sigma}(x(t)) = 0$ for u gives the equivalent control,

$$\begin{aligned}u_{eqv} = u_o - (Gg(x(t)))^{-1}Gg^\perp(x(t))g^{\perp+}(x(t))\varphi(x(t)) \\ -g^+(x(t))\varphi(x(t))\end{aligned} \tag{5.23}$$

Now, using (5.23) and (5.20),

$$\begin{aligned}\dot{x}(t) = f(x(t)) + g(x(t))u_o + g^\perp(x(t))g^{\perp+}(x(t))\varphi(x(t)) \\ -g(x(t))(Gg(x(t)))^{-1}Gg^\perp(x(t))g^{\perp+}(x(t))\varphi(x(t))\end{aligned} \tag{5.24}$$

Using (5.19b), the equation (5.24) simplifies to,

$$\dot{x}(t) = f(x(t)) + g(x(t))u_o + [I_n - \{g(x(t))(Gg(x(t)))^{-1}G\}]\varphi_u(x(t)) \tag{5.25}$$

Here I_n is identity matrix. From (5.25), it can be verified that the matched uncertainty eliminates. This implies that the sliding mode has an inherent property of elimination of the matched uncertainty. A common choice of discontinuous control u_n is,

$$u_n = -\eta(Gg(x(t)))^{-1}\frac{\sigma}{||\sigma||} \tag{5.26}$$

The system under consideration has single input. Therefore (5.26) reduces to,

$$u_n = -\eta(Gg(x(t)))^{-1}sign(\sigma) \tag{5.27}$$

Here, $sign(\sigma) = \frac{\sigma}{|\sigma|}$. Suppose the maximum upper bound of the φ_m is $\rho = ||\varphi_m||$, then by design $\eta > \rho$.

Furthermore, at $\sigma = 0$, the closed-loop uncertain dynamics model given by (5.25) contains the unmatched disturbance only (say, φ_{eqv}) given by,

$$\varphi_{eqv} = [I_n - \{g(x(t))(Gg(x(t)))^{-1}G\}]\varphi_u(x(t)) \tag{5.28}$$

In the design of ISM control, it is sufficient to choose control parameter G such that the inverse of $Gg(x(t))$ exists. However, an optimal choice of G given by (5.29) ensures that the unmatched disturbances do not amplify.

$$G = g^{+}(x(t)) = \{g^{\intercal}(x(t))g(x(t))\}^{-1}g^{\intercal}(x(t)) \tag{5.29}$$

In this example, $g(x(t)) = [z_1 x_2 \quad -z_2 x_1]^{\intercal}$ and $g^{+}(x(t)) = \left[\frac{z_1 x_2}{(z_2 x_1)^2+(z_1 x_2)^2} \quad \frac{-z_2 x_1}{(z_2 x_1)^2+(z_1 x_2)^2}\right]$. This implies $Gg(x(t)) = 1$.

The total control is $u = u_o + u_n$. This is used to generate switching pulses for the switch of front-end DC-DC boost converter. The pulses for the inverter are generated using fixed duty or open-loop unipolar sinusoidal pulse width modulation (SPWM) method.

5.4 SIMULATION RESULTS

In this Section, firstly the analysis on the ripple-reduction and dynamic performance using the conventional dual-loop control scheme is presented through simulation results. Secondly, the similar analysis is carried-out using the proposed ISM based control scheme. For the design, the system parameters given in the Table 5.1 are used.

Table 5.1 : System Parameters

Parameters	Value
Battery voltage (10 batteries each of 12 V, 26 Ah in series)	120 V
DC-link voltage	380 V
DC link capacitance and boost inductor	360 μF and 0.8 mH
Switching frequency of boost switch	25000 Hz
RMS voltage of the inverter and Modulation Index (M)	230 V ,50 Hz and $M = 0.85$
Switching frequency of inverter	5000 Hz
Control parameters $k_c = 250.$, $\zeta = 100, \beta_l = 0.075, \beta_u = 30,$ $\eta > 0.1, 10\ \mu s$/sample	

5.4.1 Analysis on Ripple-Reduction and System Dynamics Using Conventional Control

In this subsection, the analysis are presented using the conventional dual-loop control scheme. The simulation results are shown for the fixed $f_c = 1500\ Hz$ and varying the bandwidth of voltage-loop (at $f_v = 2.5\ Hz,\ 30\ Hz,\ 65\ Hz$) manually. The simulation results are shown in the Fig. 5.5. From the Fig. 5.5, it can be observed that SHC ripple in the input current of boost-derived DC-DC-DC two-stage converter decreases with the decrease in the value of f_v or k_v. However, the system dynamics are affected badly for the smaller values of f_v and k_v. This implies that a smaller bandwidth of voltage-loop results in the ripple-reduction at DC input, however, the system dynamics are poor and vice-versa. The results of the Fig. 5.5 are summarized in the Table 5.2. In Table 5.2, the SHC ripple is small in the input current for low value of k_v or f_v, however, the large over/undershoot and settling time of DC-link voltage are observed at the load-transients.

From the above analysis, it is concluded that the conventional dual-loop control has a trade-off between the ripple-reduction and dynamic performance. In the next subsection, the analysis on the ripple mitigation and dynamic performance of the system is carried-out using simulation results for the proposed adaptive PID control in the dual-loop and overall ISM based control. To design the ISM based control the adaptive PID control is used as nominal control.

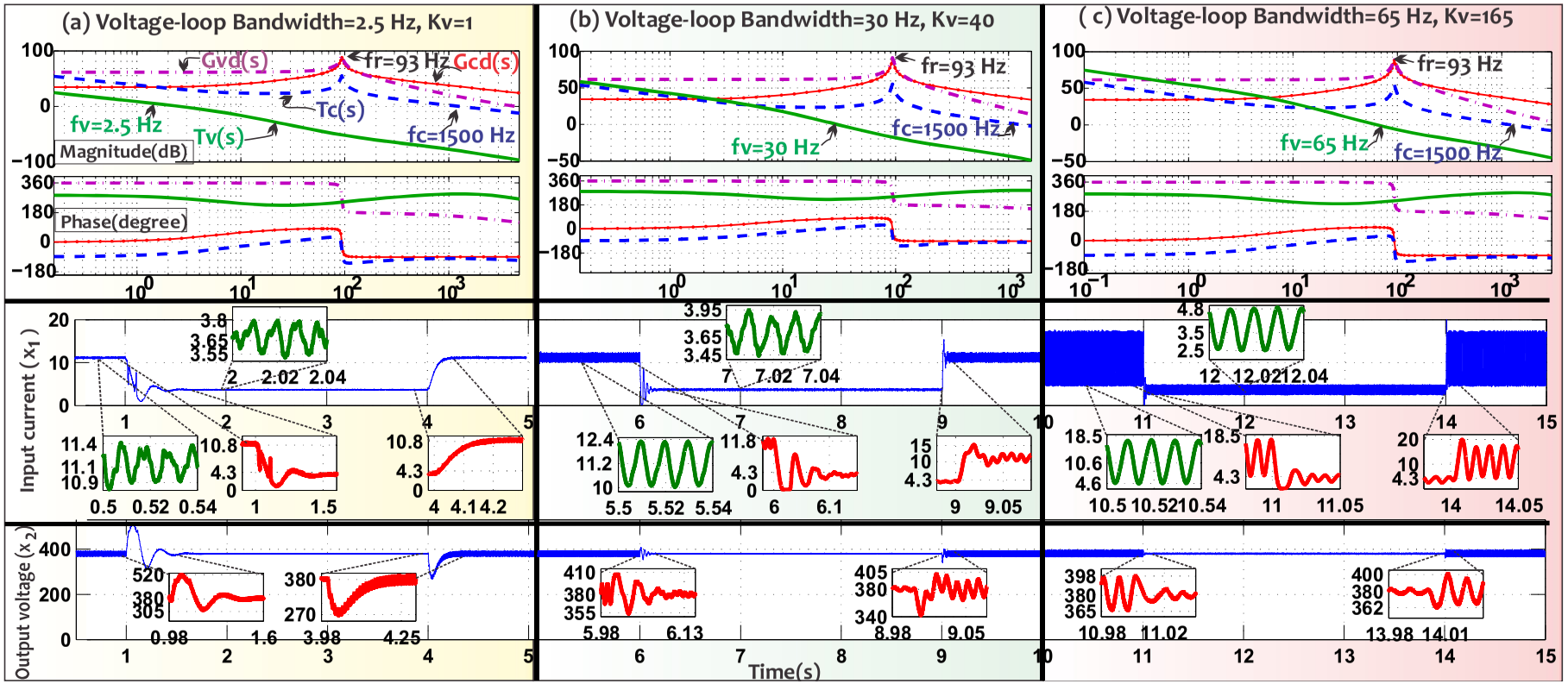

Figure 5.5 : Effect of f_v or k_v on the SHC ripple and system dynamics: SHC ripple-reduction and dynamic performance have a trade-off

Table 5.2 : Comparison of Simulation Results for Different Values of f_v (At Fixed $f_c = 1500\,Hz$)

Parameters	$f_v = 2.4Hz$	$f_v = 30Hz$	$f_v = 65Hz$
1) % SHC ripple in input current (x_1)	4.5	21	125
2) %Overshoot/Undershoot in DC-link voltage (x_2)	+37/-29	+7.9/-10.5	+4.5/-4.7
3) Settling time (ms) of x_2 at load application/ removal	600/250	130/50	20/10

5.4.2 Analysis on Ripple-Reduction and System Dynamics Using Proposed ISM Based Control

The results are presented with the adaptive PID control alone, and with ISM based control using adaptive PID control as nominal control. The analysis is carried-out for the steady-state operation and transient operation.

Case-I Steady-state operation: The Fig. 5.6(a) and Fig. 5.6(b) show the steady-state results. Firstly, the results are shown for two different cases using adaptive PID-controller alone i.e. (a) with nominal system parameters (b) with reduced size of system parameters. Using nominal size of L,C with adaptive PID-controller alone, the % peak-peak SHC ripple in input current is $< 2\%$ (see Fig. 5.6(a)). With the reduced size of L,C, the ripple increases to $> 15\%$ (see Fig. 5.6(b)). This implies that the proposed adaptive-PID controller alone minimizes SHC ripple, however, the ripple-reduction is affected by the parametric variations.

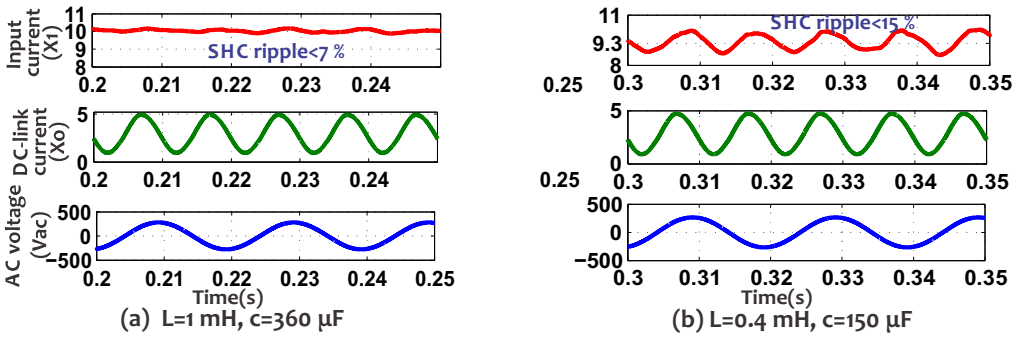

Figure 5.6 : Results with adaptive PID Control alone with (a) nominal size of L, C (b) reduced size of L, C

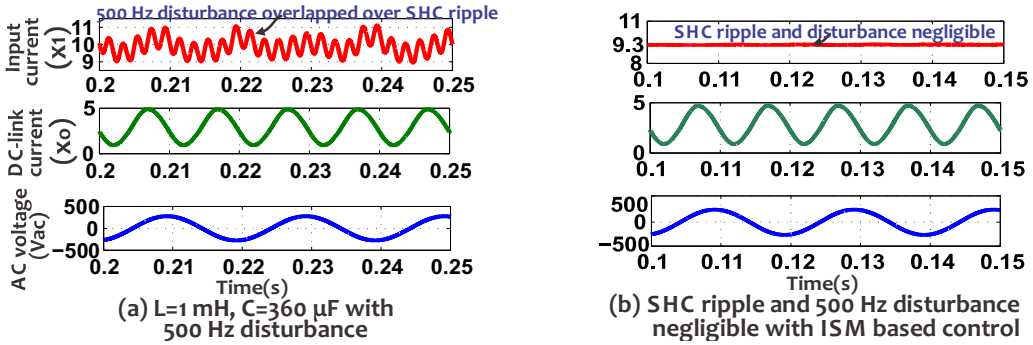

Figure 5.7 : Steady-state results of (a) adaptive PID-Controller alone and (b) proposed ISM based controller in the presence of a 500 Hz sinusoidal disturbance in duty and reduced size of L,C

Furthermore, the effect of disturbance entering through the control input with the adaptive-PID controller alone is shown in Fig. 5.7(a). A 500 Hz-sinusoidal external disturbance with magnitude 0.1 is added in the control input, this causes a similar sinusoidal disturbance in input current also (see Fig. 5.7(a)). The value of η is kept greater than 0.1 that is higher than the amplitude of sinusoidal disturbance.

Secondly, in the Fig. 5.7(b), the simulation results are shown with the ISM based control using adaptive PID control as nominal control i.e. proposed ISM based control. It is to be noted that the proposed ISM based control, not only minimizes the SHC ripple that is increased due to the reduced size of L, C in case of adaptive PID control alone but also removes the external disturbance caused by 500 Hz disturbance in the control input. This also concludes that the comparatively smaller size of L and C can be used with ISM based control.

The important feature of the proposed adaptive PID control that is used to design the ISM based control, is the improvement in dynamic performance at the large load-transients. This feature is discussed here.

Case-II Load transient operation: in the Fig. 5.8, the load transient results are shown using proposed ISM controller for 1-kW boost-derived DC-DC-AC converter. The load is varied from 100% to 10% at $t = 1\ s$ and back to 100% at $t = 2\ s$. At load reduction, the overshoot in DC-link voltage (x_2) is $< 8\%$. The voltage settles down at $x_{2r} = 380\ V$ within 500 ms. At the addition of load, the undershoot in x_2 is $< 20\%$. The non-minimum phase nature of the boost converter causes high undershoot. However, the voltage settles down at x_{2r} within 70 ms. It is to be noted the SHC ripple is negligible with the ISM proposed controller. In Fig. 5.9, the plot of switching function is shown.

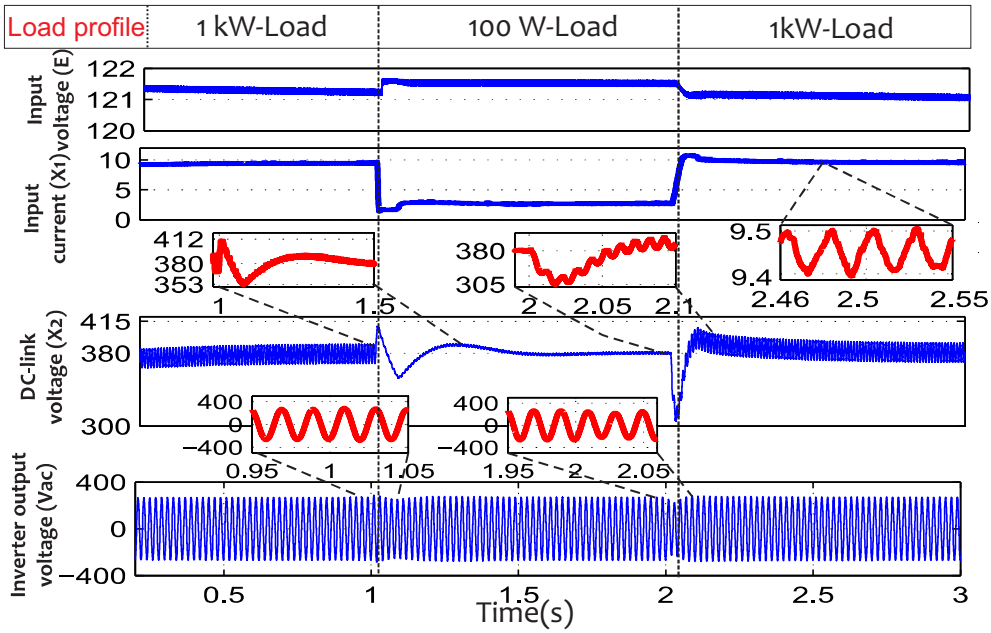

Figure 5.8 : Load transient operation results with proposed ISM based controller

In Fig.5.9, the switching function is zero at the initial time and remains so for $t > 0$.

Clearly, the proposed ISM controller suppresses the SHC ripple along with matched disturbances and improves line-load transient performance simultaneously unlike the conventional PID based dual-loop control.

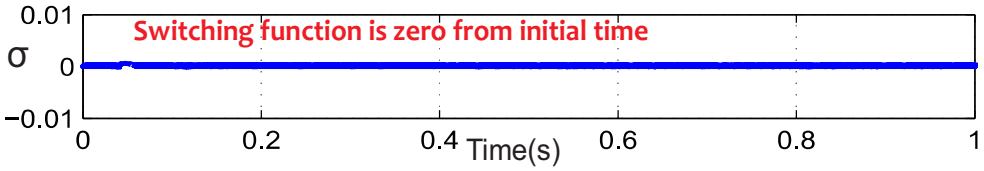

Figure 5.9 : Plot of the switching function, σ

5.5 EXPERIMENTAL RESULTS

The experimental setup is shown in the Fig. 5.10. In this figure, the battery bank, boost-derived two-stage DC-DC-AC converter, AC load and real-time digital simulator are shown. The system parameters of Table 5.1 are used for experimentation. The experimental results are shown for three different cases; CASE-I Steady-state operation, CASE-II Load transient operation and CASE-III Line transient operation.

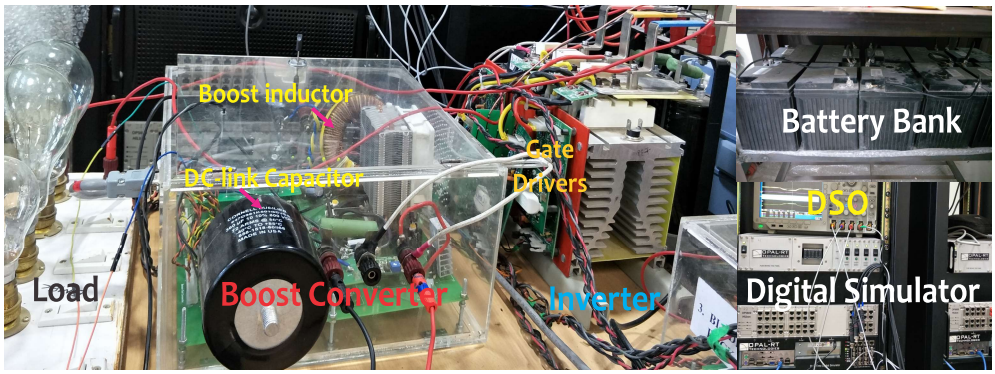

Figure 5.10 : Experimental setup of Boost-derived DC-DC-AC converter for the validation of proposed ISM based controller

Case-I: Steady-state operation The steady-state results of proposed ISM based controller are shown in the Fig. 5.11. The results are compared using proposed adaptive PID controller alone and ISM based controller. In Fig. 5.11(a), the results are shown using adaptive PID controller alone. With adaptive PID controller, the input current still has 7.7% peak-to-peak SHC ripple. This ripple reduces to negligible with ISM based controller as shown in Fig. 5.11(b). Furthermore, the steady-state results are shown by adding external disturbance in control input and by doing parametric variation in the system parameters (L, C) similar to simulation results.

1) *With parametric uncertainty:* The size of inductor is reduced from $L = 1\ mH$ to $L = 0.5\ mH$ and size of capacitor is reduced from $C = 360\ \mu F$ to $C = 100\ \mu F$. With these parametric variations, the results are shown in Fig. 5.12. It is observed that the SHC ripple in input current increases from 7.7% to 14.5% using adaptive PID control alone (see Fig. 5.12(a)). However, the ISM based control eliminates this ripple as shown in Fig. 5.12(b).

2) *With external disturbance:* In Fig. 5.13, the results are shown by adding a sinusoidal disturbance of magnitude 0.1 and frequency 500 Hz in control input. With the adaptive PID controller only, this disturbance causes a 40% peak-to-peak sinusoidal disturbance in input current (x_1) as shown in the Fig. 5.13(a).

This disturbance in x_1 is eliminated using proposed ISM based controller as shown in the Fig.

5.13(b).

Case-II: Load transient operation In Fig. 5.14, the load transients results are shown using the proposed ISM based controller. The inverter load is varied from 100% to 10% at $t = 1\ s$ and again to 100% at $t = 3.08\ s$. At the load-reduction, an overshoot of 7.5% in the DC-link voltage (x_2) from the reference voltage $x_{2r} = 380$ is observed. The voltage settles back to x_{2r} within 600 ms. At the load addition, an undershoot of 30% is observed. However, the voltage settles down to x_{2r} within 300 ms. The large undershoot is due to the non-minimum phase behavior of boost converter.

Additionally, the load-transient results for 100% load to 50% load-variation and vice-versa are shown in the Fig. 5.15. The overshoot and undershoot in the DC-link voltage (x_2) withe respect to the DC-link reference voltage are 5.2% and 13% respectively. The DC-link voltage settles back to the reference voltage in 200 ms and 120 ms at the load-reduction and at load-addition respectively.

Case-III: Line transient operation The line transient operation results using a variable unregulated rectifier supply are shown in the Fig. 5.16. The input voltage (E) is varied from 80 V to 150 V and back to 80 V. With these variations in the input voltage, the DC-link voltage is not affected and remains at reference voltage at 380 V.

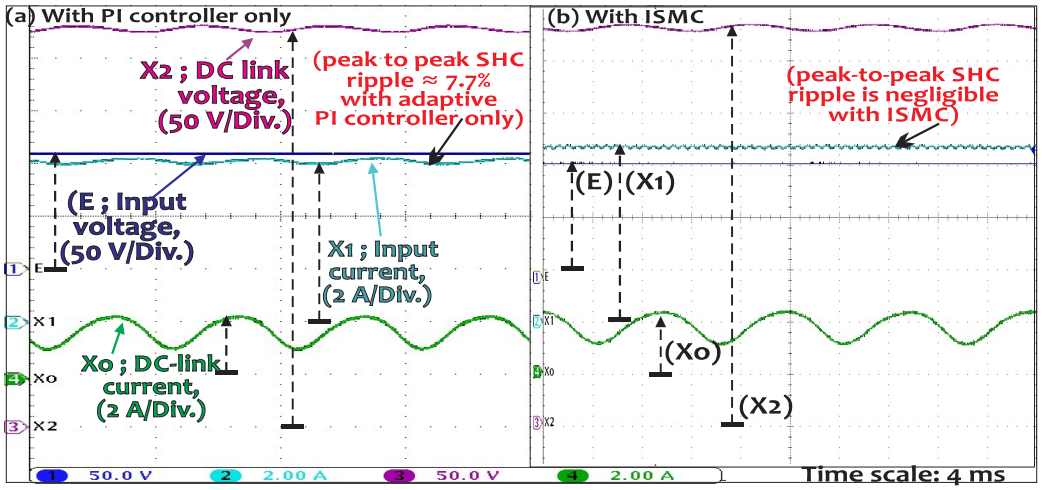

Figure 5.11 : Steady-state results with nominal size of the L and C: (a) with adaptive-PID controller alone (b) with ISM based controller

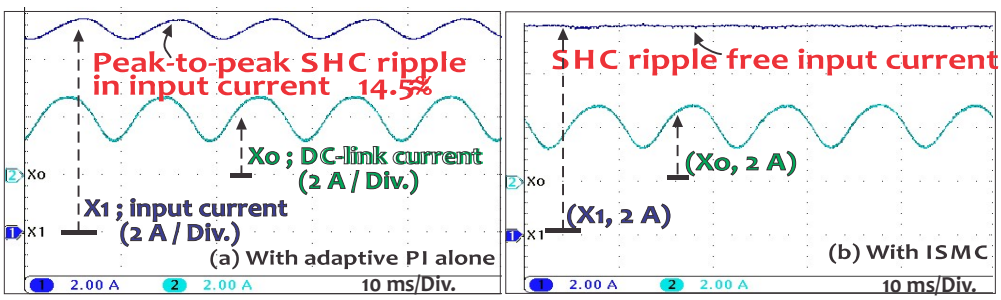

Figure 5.12 : Steady-state results with reduced size of L and C: (a) with adaptive-PID control alone (b) with ISM based control

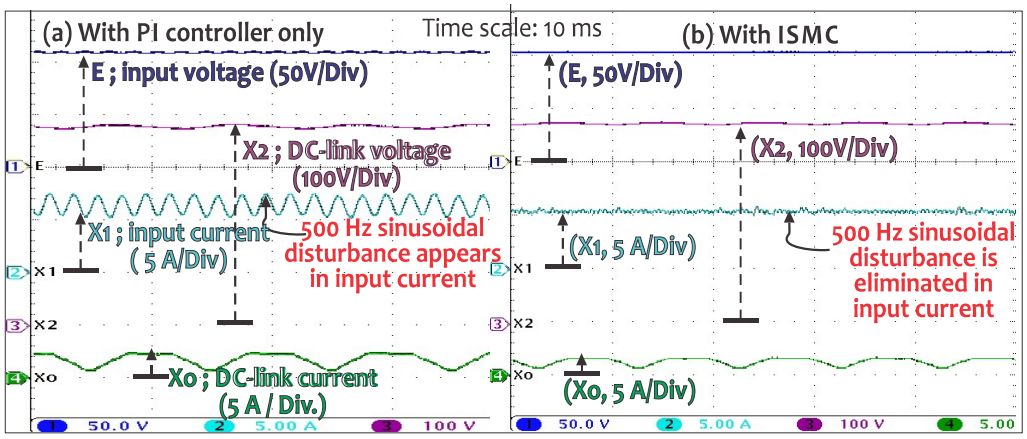

Figure 5.13 : With $500\ Hz$- sinusoidal disturbance in control input: (a) with adaptive-PID controller alone (b) with ISM based controller

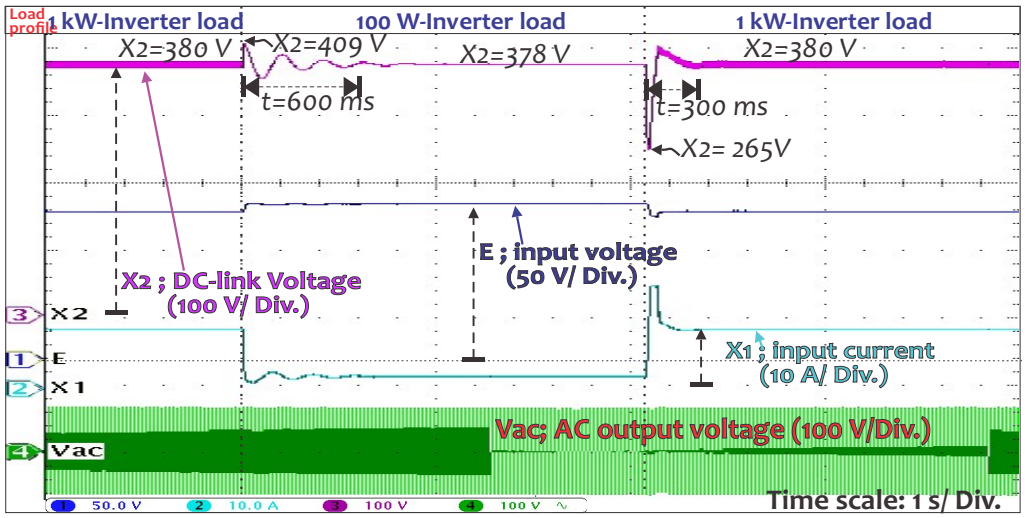

Figure 5.14 : Load transient test: load changes from 100% to 10% at $t = 1\ s$ and 10% to 100% at $t = 3.08\ s$.

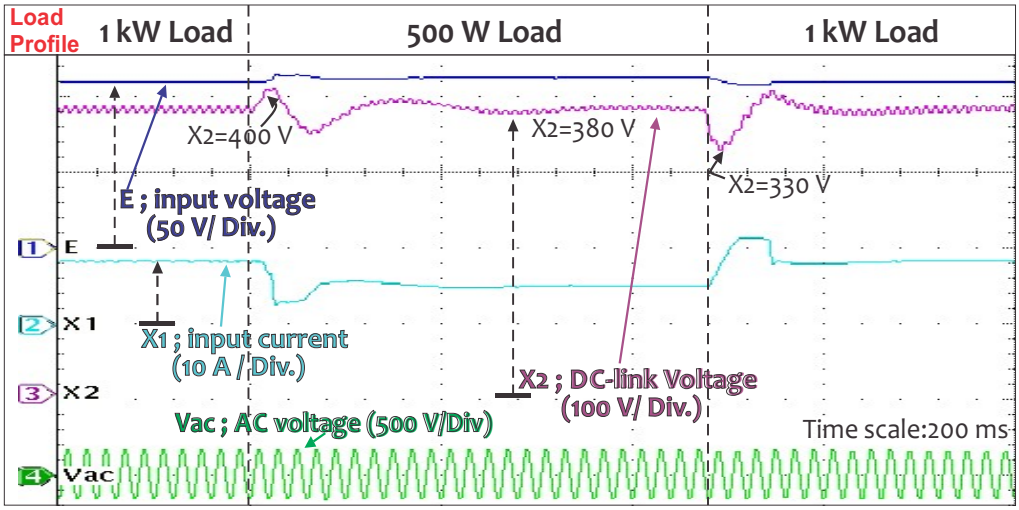

Figure 5.15 : Load transient test: load is varied form 100% to 50% at $t = 0.2\ s$ and from 50% to 100% at $t = 0.64\ s$ again.

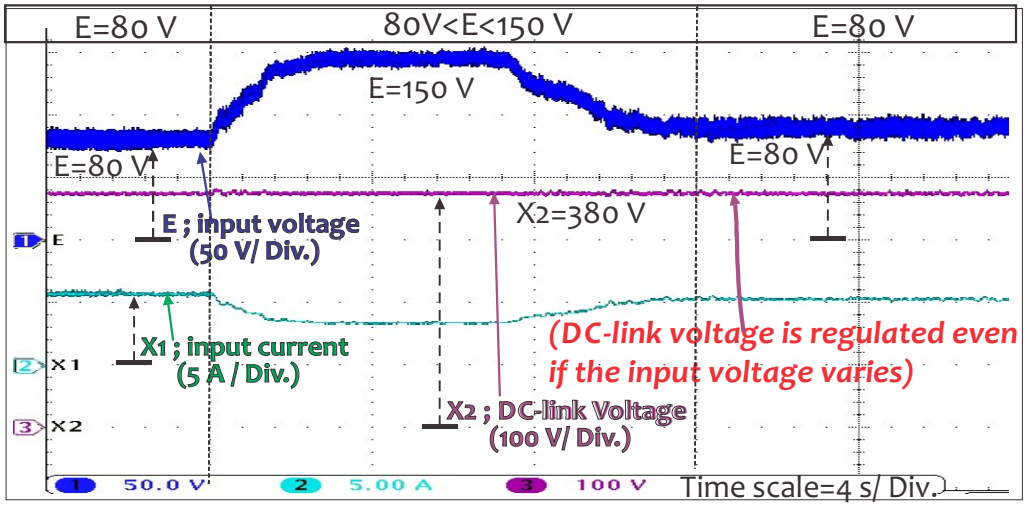

Figure 5.16 : Line transient test: input voltage is varied form 80 V to 150 V at $t = 4\ s$ and from 150 V to 80 V at $t = 11\ s$ again.

In the Table 5.3, the experimental results of the proposed controller are compared with some existing control techniques.

5.6 SUMMARY

In this Chapter, an ISM based controller has been proposed. A new adaptive PI controller for the dual-loop control has been discussed. The adaptive nature of the PI shapes the outer-loop bandwidth by self-tuning the PI gain of the outer-loop controller. The adaptive PI keeps the small value of the voltage-loop bandwidth at the steady-state and hence ripple-reduction takes place. At the line-load transients, the voltage-loop bandwidth increases monotonically to converge the system dynamics at the faster rate. The proposed ISM based controller has been validated through simulation as well as through experimentation. With the adaptive PI controller alone, the peak to peak SHC ripple at the input is less than 7.7% with respect to the average input current. The SHC ripple increases from 7.7% to 14.5% at the parametric variations. However, this ripple eliminates with the proposed ISM based controller. Furthermore, the ISM based controller also eliminates other disturbances that enter from the control input channel. At the load-transient, the DC-link voltage shows an overshoot of 7.5% and an undershoot of 30% from the nominal DC-link voltage. However, the voltage settles down within 600 s. The high undershoot is due to the non-minimum phase behavior of the front-boost converter. At the line transients, the undershoot and overshoot are negligible.

In the next Chapter, a study on the second-order ripple in the perspective of the DC micro-grid will be carried-out. In this microgrid, multiple inverter loads are considered. Furthermore, a method of phase-adjustment based ripple cancellation at the DC bus will be presented for a system having two inverters connected at DC bus.

Table 5.3 : Comparison of Proposed Control with Existing Control Schemes

Parameters	Existing control schemes Zhang *et al.* [2018b]	Proposed ISMC
(1) Power rating, input voltage, DC-link voltage and capacitance	$1-kW,\ 110\pm10\%\ V,\ 380\ V,$ $810\mu F$	$1-kW,\ 120\pm30\%,\ 380\ V,$ $360\mu F$
(2) %Δ SHC ripple in input current (x_1) at Steady-state	5% (VRS), 5% (BPF+ICFS), 5% (NF-LCFFS), 3% (NF-VR+LCFFS)	Negligible with proposed ISMC
(3) % overshoot/undershoot in x_2 at Line-transients	Not available	Negligible
(4) % overshoot/undershoot in DC-link voltage (x_2) at Load-transients	$+9.26/-10.4$ (VRS), $+3.26/-4.42$ (BPF+ICFS), $+2.1/-3.58$ (NF-LCFFS), $+2/-3.3$ (NF-VR+LCFFS)	$+7.5/-30$
(5) Robustness Analysis	Not available	Eliminates disturbances

Virtual Resistor-Based Control Scheme (VRS), Notch Filter-Inserted Load-Current Feedforward Scheme (NF LCFFS), Bandpass Filter Incorporated Diode Current Feedback Scheme (BPF-DCFS/BPF-ICFS), Notch-Filter Cascading Voltage Regulator Plus Load Current Feedforward Scheme (NF-VR+LCFFS)